A Sea-Level Control on the Eruptive Activity of Santorini Volcano, Greece

C. Satow[1]*, A. Gudmundsson[2], R. Gertisser[3], C. Bronk Ramsey[4], M. Bazargan[5], D. M. Pyle[6], S. Wulf[7], A.J. Miles[8], M. Hardiman[7].

[1]*Department of Humanities and Social Sciences, Oxford Brookes University, Headington Road, Oxford, United Kingdom.*
[2]*Department of Earth Sciences, Royal Holloway University, Egham, Surrey, United Kingdom*
[3]*School of Geography, Geology and the Environment, Keele University, Keele, United Kingdom*
[4]*Research Laboratory for Archaeology and the History of Art, University of Oxford, 1 South Parks Road, Oxford, United Kingdom*
[5]*Department of Earth Sciences, Uppsala University, Villavägen 16, Uppsala, Sweden*
[6]*Department of Earth Sciences, University of Oxford, South Parks Road, Oxford, UK*
[7]*School of the Environment, Geography and Geosciences, University of Portsmouth, Portsmouth, United Kingdom*
[8] *School of Geography, Geology and the Environment, University of Leicester, University Road, Leicester, UK*
**correspondence: csatow@brookes.ac.uk*

Abstract

Sea-level change is thought to modulate the frequencies of volcanic eruptions on glacial to interglacial timescales, but the underlying physical process is poorly understood. Here we compare a ~360 kyr long record of effusive and explosive eruptions from the flooded caldera volcano at Santorini, Greece, with a high resolution sea-level record spanning four glacial-interglacial cycles. Numerical modelling shows that when the sea level falls by 40 m below the present-day level, the induced tensile stresses in the roof of the magma chamber of Santorini trigger dyke injections. At -40 m, however, all injected dykes become arrested, and no eruptions occur. As the sea-level continues to fall to -70 or -80 m, the induced tensile stress spreads throughout the roof so that some dykes reach the surface to feed eruptions. Similarly, the volcanic activity gradually disappears once the sea-level rises above -40 m. Synchronising Santorini's stratigraphy with the sea-level record by using tephra layers in marine sediment cores shows that 208 out of 211 eruptions occurred during periods when the sea-level was at -40 m or lower, suggesting a strong absolute sea-level control on the timing of eruptions on Santorini – a result that probably applies to many other volcanic islands around the world.

Climate as a Driver of Volcanism

The climate system's influence on solid-earth processes, including volcanic and tectonic activity[1-4] is receiving increasing attention from researchers. Changes in surface loading by growth and retreat of ice-sheets have been linked to changes in volcanic activity in formerly glaciated areas on timescales from 10^3 - 10^6 years[5-11]. Removal of an ice-sheet reduces the overburden pressure and results in additional decompression melting in the mantle. The associated stress changes in the crust facilitate dyke propagation to the surface, thereby increasing volcanic activity[10]. The effects of concomitant sea-level changes on volcanic activity, however, have not yet been firmly established. Because sea-level change is a worldwide phenomenon and the majority of the earth's volcanic systems are located in or next to oceans, this effect is of great global concern.

Previous studies of the effect of sea-level change on subaerial volcanic systems have been based only on ash layers preserved in marine sediment cores[12-14]. These studies have identified periods of greater eruptive activity that appear cyclical on Milankovitch timescales of 41 and 100 kyr [13,14]. Most

volcanic systems, however, are not dominated by large explosive, ash-producing eruptions but by lava effusion and/or minor explosive activity, neither of which are represented in marine sediment core records. As a result, no studies have yet been able to compare the full range of eruptive activity from a single subaerial volcano to a sea-level record. The physical mechanisms that could link changes in sea-level and volcanic activity also remain elusive, with periods of increased explosive activity variously attributed to high rates of sea-level change[12], absolute sea-level changes through Milankovitch cycles[13-16], or increased melt production in the mantle[17].

To correlate sea-level changes with volcanic activity requires a well-dated volcanic system with a long and detailed proximal and distal record of both explosive and effusive eruptions, extending over more than one glacial-interglacial sea-level cycle. Santorini volcano, Greece (Supplementary Figure 1), satisfies all of these requirements. It has an unusually long, precisely dated and accessible record of major explosive (Plinian) eruptions and chronologically well-constrained intervals of lava effusion and minor explosive (interplinian) eruptions[18-20]. Santorini also benefits from the exceptional chronological control afforded by ash layers preserved in nearby marine sediment cores[21,22] (Supplementary Figure 1). Crucially for this study, these ash layers have been dated[22] with the same chronology as a recent, global sea-level curve[23,24], allowing direct alignment of the volcanic stratigraphy to the sea-level record and ensuring the most precise synchronisation of the two records possible.

The eruption time series for Santorini

Figure 1 shows the detailed eruption chronology of Santorini from ~360 ka to the present day. On the basis of long-term trends in magma composition, the eruption history has traditionally been split into two cycles[18,25.] Each cycle starts with effusive eruptions of low or intermediate silica content and ends with major silicic eruptions and a caldera collapse. The volcano is now, after the famous Late Bronze Age eruption[26,27], in its third cycle. These cycles are recorded in detail by the stratigraphy of the caldera walls (the islands of Thira and Thirasia, Supplementary Figure 1), where deposits originating from twelve major explosive (Plinian) eruptions, minor explosive (interplinian) eruptions and lava eruptions are evident.

A detailed chronology for the volcano[18,22,25] reveals long periods of quiescence which are marked by palaeosols and a notable absence of volcanic deposits (Fig. 1). While studies have explored magma-system controls on the nature of individual eruptions[26,28,29] , the factors controlling the start and end of eruptive and quiescent phases have not been determined. Internal forcing such as increased magma flux into a magma chamber or external forcing such as the changes in crustal loading during glacial-interglacial cycles[13-16,30] may both play a role, but the relative importance of those roles has not yet been established.

Geophysical, petrological and geochemical results provide compelling evidence for the existence of a shallow magma chamber at the depth of about 4 km beneath Santorini's caldera[19,25,29,31-35]. To simulate the influence of sea-level loading, we present the results of numerical modelling (Fig. 2; Supplementary Figure 2) which indicate that stress changes due to changes in sea-level during the Late Quaternary are sufficient to trigger (during low sea-level) or inhibit (during high sea-level) dyke injection from the magma chamber. We test our model results by integrating Santorini's volcanic stratigraphy with a eustatic sea-level record[23,24] (and also rates of sea-level change- Supplementary Figure 3) spanning four glacial-interglacial cycles. The empirical evidence supports our model,

suggesting that eustatic sea-level-induced stress changes over the past 360 kyr largely controlled dyke injections from the shallow chamber and, therefore, the timing of periods of eruptive activity.

Modelling the effect of sea-level changes on dyke injection and eruptions

When global sea-level rises, the load on the crust/lithosphere increases; when the sea-level falls, the load decreases. The load here is the vertical stress due to the hydrostatic pressure of the sea water. Hydrostatic pressure p is given by $p = \rho g z$ where ρ is the water density, g is the acceleration due to gravity, and z is the depth below the surface of the water. Using the average sea-water density of 1025 kgm^{-3} and the acceleration due to gravity of 9.8 ms^{-2}, it follows that for every 10 m that the sea-level rises/falls the hydrostatic pressure or vertical stress changes by about 0.1 MPa, which translates into changes in crustal stresses[36,37] . In the vicinity of a magma chamber, increases in horizontal compressive stresses tend to inhibit, while increases in horizontal tensile stresses encourage, dyke injections from the chamber[37]. Rock tensile strength is almost constant to a crustal depth of 9 km (mostly 1-6 MPa, with an average of about 3.5 MPa[36]), so we assume that it does not vary in our model. If (as at Santorini) the crust hosts a shallow magma chamber the tensile stresses induced by sea-level fall become magnified (Fig. 2).

To simulate the effect of sea-level changes on the potential for dyke injections and eruptions, we used the software Comsol Multiphysics (www.comsol.com) to model associated changes in tensile stress concentration around the shallow magma chamber of the Santorini volcano. To explore how the tensile stress concentration in the roof of the chamber (controlling dyke propagation) changes during the fall in sea-level, we decreased the vertical stress in steps of 0.1 MPa, corresponding to sea-level falls of 10 m. This is the only loading in the model runs. Using the contemporary mean sea-level as the starting point (0 m), the final sea-level in the model is the one associated with the last glacial maximum at ~22 ka, namely -110 m. The initial (0 m) and final (-110 m) levels cover the entire range of Quaternary sea-level changes. We model the shallow magma chamber at 4 km depth as a 6 km-wide (horizontal dimension) sill-like flat ellipsoid and initially (at 0 m sea-level, the starting point in the model) in lithostatic equilibrium with the host rock. These assumptions as to geometry and lithostatic equilibrium are in line with geophysical observations[34,35] and previous magma-chamber modelling studies[28,37]. In the model, the crust hosting the chamber is layered (Fig. 2). We use typical 'seismic' layers, each 500 m thick and with increasing stiffness (Young's modulus) with depth, as is normal in volcanic areas[37].

The modelling results (Fig. 2) show how the induced tensile stress gradually spreads from the margin of the chamber and throughout the entire roof up to the surface as the sea-level falls in steps of 10 m from its initial (0 m) to its lowest (-110m) level. Dyke injection from a chamber occurs when the following condition is satisfied: $p_l + p_e = \sigma_3 + T_0$, where p_l is the lithostatic pressure, p_e is the magmatic excess pressure in the chamber with reference to σ_3, the minimum compressive principal stress in the roof next to the chamber, and T_0 is the in-situ (field) tensile strength of the roof[37]. Initially the chamber is in lithostatic equilibrium with the host rock, so that p_e is zero and no dykes are injected. As the sea-level falls, tensile-stress concentration around the chamber reduces σ_3 thereby increasing p_e. When the excess pressure p_e reaches the tensile strength of the roof, T_0, the roof ruptures and a dyke is injected. Using the average tensile strength of 3.5 MPa, the excess pressure p_e must reach that value for a dyke to be injected.

The numerical modelling (Fig. 2; Supplementary Figure 2) shows that the tensile stress in the roof next to the chamber, hence p_e, reaches the absolute value of 3.5 MPa when the sea-level has fallen to about -40 m (40 m below the current level). Thus, magma-chamber rupture and dyke injection is encouraged once the sea-level has fallen by 40 m. At this sea-level, however, the tensile stress is limited to the vicinity of the chamber; away from the chamber there is no tensile stress concentration. Consequently, at this stage the injected dykes become arrested close to the magma chamber and do not reach the surface to supply magma to eruptions[37]. As the sea-level continues to fall below -40 m, however, the induced tensile stress gradually spreads throughout the entire roof of the magma chamber. There is therefore an expected time-lag between the first dykes injected during a sea-level fall and the first dyke-fed eruptions at the surface (Figs. 2 and 3). Quantifying and explaining this time-lag is important in order to establish a complete understanding of how volcanism at Santorini, and subsequently other volcanic islands, reacts to sea level changes.

A time-lag between first sea-level triggered dyke injections and first dyke-fed eruptions

Time-lags between external forcing and volcanic response have been inferred in many previous studies. For basaltic volcanism in eastern California, the lag between glacial unloading and peak volcanism is defined as 11.2± 2.3 kyr[7]. Also, the peak explosive volcanism in the Izu Bonin Arc (western Pacific Ocean) apparently lags behind the glacial maximum (sea-level minimum) by approximately 7 kyr[15]. Similarly, in Iceland the peak in late glacial and early Holocene volcanism occurred several thousand years after the deglaciation began[5, 10]. Some of these time-lags have been attributed to viscoelastic behaviour of the crust. However, the response of a crustal segment hosting a magma chamber is normally elastic to a first approximation[37-40]. Thus, volcanic eruptions usually occur during unrest (inflation/deflation) periods[37] rather than hundreds or thousands of years after the unrest took place. Viscoelastic behaviour of the crust[17], therefore, cannot be used to explain the long time-lags commonly observed between large-scale (glacial or sea-level) unloading of the crust in volcanic areas and subsequent peaks in the numbers of eruptions.

Our model (Figs. 2 and 3) indicates instead that such a long time-lag is a direct consequence of the evolution of the stress field in the roof of the magma chamber during the gradual change in external loading (Figs. 2 and 3). When the sea-level falls to -40 m, induced tensile stress concentration encourages dyke injection and propagation into the lower part of the roof of the chamber (Figs. 2 and 3). However, the stress in the upper part of the roof, closer to the surface, is still unfavourable to dyke propagation, so that the dykes become arrested (cf. 37, 40). As the sea level continues to fall further, greater parts of the roof become subject to tensile stress (Figs. 2 and 3) so that the probability of an injected dyke reaching the surface to erupt increases. Similarly, when the sea level rises again, the tensile stresses gradually become suppressed (not shown in Fig. 2) until sea-level triggered dyke injections stop. There is thus an expected time-lag between the initiation of sea-level induced local stress fields favourable/unfavourable to dyke injections and the initiation/suppression of dyke-fed eruptions.

For Santorini, this time-lag can be quantified by using the period of eruptive activity (Fig. 4) constrained between the Plinian Lower Pumice 2 eruption at 176.7 +/- 0.6 ka[20] and the interplinian M9-2 eruption at 121.8 +/- 2.9 ka[22]. This eruption period is used not only because of the very precise dates defining its start and end[22], but also because these eruption dates are defined using ash layers

in marine sediment cores (Supplementary Figure 1) which share the same chronology as the sea-level record[22-24], thereby eliminating the chronological uncertainty which would be otherwise be introduced by aligning two separate chronologies.

Sea-level drops below -40 m (when dyke-injection begins; Figs. 2 and 3) at 189.5 +/- 2.4 ka (Fig. 4) and rises back through -40 m at 132.5 +/- 2.1 ka[24]. The time-lag between the sea-level falling below -40 m and the start of eruptive activity marked by the Lower Pumice 2 eruption at 176.7 +/- 0.6 ka[20] is therefore 12.8 +/- 2.5 kyr. Eruptions in Santorini's volcanic record normally began when the sea-level had fallen by 70-80 m below that of the present day (Fig. 4). Our model results (Figs. 2 and 3) show that this is the level at which the induced tensile stress had spread through much of the roof of the shallow chamber, meaning that propagation of injected dykes is encouraged in most of the roof. The time-lag of 12.8 +/- 2.5 kyr associated with sea-level falling therefore reflects the time it usually takes for the sea-level to fall from -40 m to –70 m or -80 m (Figs. 3 and 4). At -40 m the injected dykes become arrested, and no eruptions occur. At -70 or -80 m the sea-level tensile stress is so widespread in the roof that some dykes reach the surface to feed eruptions (Fig. 3).

Similarly, the time-lag between the sea-level rising above -40 m and the end of eruptive activity marked by the M9-2 eruption at 121.8 +/- 2.9 ka is 10.7 +/- 3.6 kyr. The rise in sea-level is much faster (Fig. 4) and thus at a higher strain rate than the fall. In addition, during the rise above -40 m (but not during the fall below -40 m) there exist recently formed feeder-dykes (Fig. 3), some of which are still hot and perhaps partly molten close to the chamber. This combination of high strain rate and hot/partly molten dyke rock results in tensile stress concentrations that encourage dyke-fed eruptions even after the sea-level has risen above -40 m. Feeder-dykes formed under these conditions may be multiple (repeatedly using essentially the same path), particularly close to the chamber. This explains the observed 10.7 +/- 3.6 kyr time lag between the sea-level rising through the -40 m threshold and the cessation of eruptive activity at the surface (Fig. 4). As the sea-level approaches the current level (0 m), however, the tensile stresses become suppressed and dyke-fed eruptions eventually cease (Fig. 4).

Because the time-lags associated with sea level rising (10.7 +/- 3.6 kyr) and sea level falling (12.8 +/- 2.5 kyr) are so similar (within uncertainties roughly between 7 and 15 kyr) we calculate a single, mean time-lag (the time between the -40m sea level and the start or end of periods of eruptions) for Santorini of 11.8 +/- 1.9 kyr (Fig. 4). We then test this time-lag across the entire 360 kyr record of volcanic activity at Santorini in Figure. 4.

Periods of eruptive activity constrained by a sea-level threshold

Our numerical results of sea-level induced stress changes around Santorini's shallow magma chamber (Figs. 2 and 3) indicate that eruptive activity will start 11.8 +/- 1.9 kyr after the sea level has fallen below -40 m (when the sea-level is at -70 m or -80 m) and cease about 11.8 +/- 1.9 kyr after sea level has risen above -40 m. Figure 4 shows that all but 3 of the 211 deposits (of all eruptive styles; Plinian, interplinian and lava) counted within the Santorini stratigraphy (between 224 ka and the present day) were erupted during such periods. Only one minor (interplinian) and two major (Plinian) explosive eruptions occurred outside of these periods. This pattern also appears to extend to the older and less well preserved part of Santorini's volcanic record (older than 224 ka, Fig. 4) where it is not possible to quantify the exact number of eruptions, or the dating is less precise. Prior to 224 ka, all known eruptions occurred during such periods. The lack of evidence for eruptive

activity outside of these periods indicates that absolute sea-level exerts a fundamental control on the timing of eruptions at the Santorini volcano, by modulating the tensile stress and therefore dyke propagation above the magma chamber.

Implications for volcanic hazards

Cycles in eruptive composition and behaviour have long been recognised at Santorini[18,25] with the second explosive cycle culminating in the famous Late Bronze Age, or Minoan, eruption. The volcano is now considered to be at the start of its third cycle (Figs 1 and 4) and minor, effusive interplinian eruptions are thought to be the most likely hazard[25,31,43]. Our new analysis adds considerably to the understanding of these cycles by revealing that the timing of periods of eruptions is primarily controlled by changes in sea-level. This in turn indicates that the volcano will shortly enter a period of long-term repose. Sea-level last rose through -40 m at 11.2 +/- 0.7 ka[23,24] and the time-lag between this sea-level and cessation of minor (effusive) eruptions (lava and interplinian in Fig. 4) is estimated here to be 11.8 +/- 1.9 kyr. Santorini volcano is therefore currently within the uncertainty range of this study's predicted cessation of effusive eruptive activity. It has been dormant since the 1950 eruption of Nea Kameni[25,41,42] (Fig. 1) and magma injected into the Santorini magma chamber in 2011-2012[34,41-43] failed to cause an eruption, hinting that this period of quiescence may already have begun. However, the eruptive record (Fig. 4) shows that two major explosive 'Plinian' eruptions (Cape Therma 3 and Lower Pumice 1; Fig. 1) occurred outside periods subjected to sea levels of below -40 m (with a 11.8 +/- 1.9 kyr time-lag) and therefore that such large eruptions may remain a present-day threat. Nonetheless, the timing of 208 out of 211 eruptions recorded in the highly detailed volcanic stratigraphy at Santorini can be explained by the mechanism of dyke injection and propagation resulting from the tensile stresses induced by low sea levels.Around 57% of the world's sub-aerial volcanoes are islands or on coasts[12], and therefore potentially affected by sea-level induced stress changes. The precise effects of sea-level changes on any particular volcanic system will depend on the geometry and depth of the source magma chamber and the mechanical properties of the crustal segment hosting the chamber. Comparative studies of other systems are vital to provide a general framework for making individual volcanic hazard assessments[14]. Such assessments are, understandably, often set within the context of past eruptive behaviour and timing. This study, however, implies that the unusually stable sea level of the Holocene and likely sea-level rise in the future (due to anthropogenic climate change) may render simple extrapolation of past eruption patterns, timings and styles into the future inaccurate. Instead, the eruptive history of any volcanic systems where sea-level variations may induce local stress-field changes should be examined within the context of a sea-level record to better infer their likely future eruptive behaviour.

The precise and detailed chronology of the Santorini volcano has allowed us, for the first time, to establish a clear relationship between sea-level change and the timing of the eruptions of an active, subaerial volcano. Our results should encourage all island volcanic systems around the world to be examined within the context of sea-level induced stress changes around active magma chambers.

Acknowledgements and funding

CBR received funding from NERC in support of the NERC Isotope Facility. DMP acknowledges support from the NERC Centre for the Observation and Modelling of Earthquakes, Volcanoes, and Tectonics

(COMET). MB acknowledges financial support from the Swedish Research Council (2018-03414) and the Weld On Sweden Research and Development Section. CS dedicates this paper to Amy and Rory.

References

1. Matthews, R.K. Tectonic implications of glacio-eustatic sea-level fluctuations. *Earth Planet. Sci. Lett.* **5**, 459–462 (1969).

2. Rampino, M. R., Self, S. & Fairbridge, R. W. Can rapid climate change cause volcanic eruptions? *Science* **206**, 826–828 (1979).

3. Paterne, M. and Guichard, F. Triggering of volcanic pulses in the Campanian area, South Italy, by periodic deep magma influx. *J. Geophys. Res.* **98**, 1861-1873 (1993).

4. Mason, B.G. et al. Seasonality of volcanic eruptions, *J. Geophys. Res.* **109**, B04206 (2004).

5. Gudmundsson, A. Mechanical aspects of postglacial volcanism and tectonics of the Reykjanes Peninsula, southwest Iceland. *J. Geophys. Res*. **91**, 12,711-12,721 (1986).

6. Jull, M. and McKenzie, D. The effect of deglaciation on mantle melting beneath Iceland. *J. Geophys. Res*. **101**, 21815-21828 (1996).

7. Jellinek, M.A., Manga, M., and Saar, M. Did melting glaciers cause volcanic eruptions in eastern California? Probing the mechanics of dike formation. *J. Geophys. Res*. doi:10.1029/2004JB002978 (2004).

8. Nowell, D.A.G., Jones, M.C. and Pyle, D.M. Episodic Quaternary Volcanism in France and Germany. *J. Quat. Sci*. **21**, 645-675 (2006).

9. Watt, S.F.L., Pyle, D.M. and Mather, T.A. The volcanic response to deglaciation: evidence from glaciated arcs and a reassessment of global eruption records. *Earth Sci. Rev.* **122**, 77-102 (2013).

10. Andrew, R.E.B., Gudmundsson, A. Distribution, structure, and formation of Holocene lava shields in Iceland. *J. Volcanol. Geotherm. Res*., **168**, 137-154 (2007).

11. Rawson, H. et al. The magmatic and eruptive response of arc volcanoes to deglaciation: insights from southern Chile. *Geology* **44**, 251-254, doi:10.1130/G37504.1 (2016).

12. McGuire et al. Correlation between rate of sea-level change and frequency of explosive volcanism in the Mediterranean. *Nature* **389** pp473-476 (1997).

13. Kutterolf, S. et al. A detection of Milankovitch frequencies in global volcanic activity. *Geology* doi:10.1130/G33419.1 (2012).

14. Kutterolf, S. et al. Milankovitch frequencies in tephra records at volcanic arcs: The relation of kyr-scale cyclic variations in volcanism to global climate changes. *Quart. Sci. Rev.* **204**, 1-16 (2019).

15. Schindlbeck et al. 100 kyr cyclicity in volcanic ash emplacement: evidence from a 1.1 Myr tephra record from the NW Pacific. *Scientific Reports* DOI:10.1038/s41598-018-22595-0 (2018).

16. Stewart, I.S. Did sea-level change cause the switch from fissure-type to central-type volcanism at Mount Etna, Sicily? *Episodes* **41**, 7-16 (2018).

17. Sternai, P., et al. Magmatic pulse driven by sea-level changes associated with the Messinian salinity crisis. *Nat. Geo.* DOI: 10.1038/NGEO3032 (2017).

18. Druitt.T.H et al. Explosive volcanism on Santorini, Greece. *Geol. Mag.* **126,** 95-126 (1989).

19. Druitt, T.H., Pyle, D.M. and Mather, T.A. Santorini Volcano and its Plumbing System. *Elements* **15**, 177-184, doi: 10.2138/gselements.15.3.177 (2019).

20. Satow et al. Detection and Characterisation of Eemian Marine Tephra Layers within the Sapropel S5 1 Sediments of the Aegean and Levantine Seas. *Quaternary* **3** doi:10.3390/quat3010006 (2020)

21. Satow et al. A new contribution to the Late Quaternary tephrostratigraphy of the Mediterranean; Aegean Sea core LC21. *Quart. Sci. Rev.* **117***,* 96-112 (2015).

22. Wulf, S. et al. Advancing Santorini's tephrostratigraphy: new glass geochemical data and improved marine-terrestrial tephra correlations for the past ~360 kyrs. *Earth Sci. Rev*. https://doi.org/10.1016/j.earscirev.2019.102964 (2020).

23. Grant et al. Rapid coupling between ice volume and polar temperature over the past 150,000 years. *Nature* **491**, 744-747 (2012).

24. Grant et al. Sea-Level variability over 5 glacial cycles. *Nat. Commun.* **5** 5076 DOI: 10.1038/ncomms6076 (2014).

25. Druitt, T.H., et al. Santorini volcano. *Geol. Soc. Lond*. Mem. **19**, 1-165 (1999).

26. Druitt et al. Decadal to monthly timescales of magma transfer and reservoir growth at a caldera volcano. *Nature* doi:10.1038/nature10706 (2012).

27. Nomikou, P et al. Post-eruptive flooding of Santorini caldera and implications for tsunami generation. *Nature Commun.* DOI: 10.1038/ncomms13332 (2016).

28. Browning**.** et al. Forecasting magma chamber rupture at the Santorini Volcano, Greece *Nature Sci. Rep.* **5, 15785 DOI: 10.1038/srep15785** (2015).

29. Fabbro, G.N., Druitt, T.H. and Costa, F. Storage and eruption of silicic magma across the transition from dominantly effusive to caldera-forming states at an arc volcano (Santorini, Greece). *J. Petrol.* **58**, 2429-2464 (2017).

30. Wallman, P., Mahood, G. A., and Pollard, D.D. Mechanical models for correlation of ring fracture eruptions at Pantelleria, Strait of Sicily, with glacial sea-level drawdown. *Bull. Volcanol.* **50**, 327-339 (1988).

31. Parks, M.M., Biggs, J., England, P., Mather, T.A., Nomikou, P., Palamartchouk, K., Papanikolaou, X., Paradissis, D., Parsons, B., Pyle, D.M., Raptakis, C., Zacharis, V. Evolution of

319 Santorini volcano dominated by episodic and rapid fluxes of melt from depth. Nature Geoscience
320 5, 749-754 (2012)

321 32. Hooft et al. Seismic imaging of Santorini: Subsurface constraints on caldera collapse and
322 present-day magma recharge*. Earth. Planet. Sci. Lett*. **514**, 48-61 (2019).

323 33. Druitt, T.H. et al. Magma storage and extraction associated with Plinian and interplinian
324 activity and Santorini Caldera (Greece) *J. Petrol.* **57,** 461-494 (2016).

325 34. Parks, M.M., et al. From quiescence to unrest - 20 years of satellite geodetic measurements
326 at Santorini volcano, Greece. *J. Geophys. Res.* (Solid Earth), **120**, 1309-1328,
327 doi:10.1002/2014JB011540 (2015).

328 35. McVey et al. Magma accumulation beneath Santorini volcano, Greece, from P-wave
329 tomography. Geology **48:** 231-235 (2020).

330 36. Gudmundsson, A. Rock fractures in geological processes. Cambridge University Press,
331 Cambridge (2011).

332 37. Gudmundsson, A. *Volcanotectonics: Understanding the structure, deformation and dynamics*
333 *of volcanoes* (Cambridge Univ. Press, Cambridge, 2020).

334 38. Dzurisin, D. *Volcano deformation: new geodetic monitoring techniques* (Springer Verlag,
335 Berlin, 2006).

336 39. Segall, P. *Earthquake and volcano deformation*. Princeton Univ. Press, Princeton, 2010).

337 40. Gudmundsson, A. Emplacement and arrest of dykes and sheets in central volcanoes. *J.*
338 *Volanol. Geotherm. Res.* **116**, 279-298 (2002).

339 41. Parks, M.M. et al. Evolution of Santorini volcano dominated by episodic and rapid fluxes of
340 melt from depth. *Nature Geosci*. **5**, 749-754 (2012).

341 42. Parks, M.M. et al. Distinguishing contributions to diffuse CO_2 emissions in volcanic areas from
342 magmatic degassing and thermal decarbonation using soil gas ^{222}Rn-$\delta^{13}C$ systematics: application
343 to Santorini volcano, Greece. *Earth Planet. Sci. Lett*. **377-378**, 180-190 (2013).

344 43. Newman et al. Recent geodetic unrest at Santorini Caldera, Greece. *Geophys. Res. Lett.* **39**
345 doi:10.1029/2012GL051286 (2012).

346 44. Edwards, L., Magma cyclicity and isotopic variation on Santorini volcano, Aegean Sea,
347 Greece. Ph.D. Thesis University of Bristol, UK (1994).

348 45. Vespa.M et al. Interplinian explosive activity of Santorini volcano (Greece) during the past
349 150,000 years. *J Volcanol. Geotherm. Res.* **153,** 262-286 (2006).

350 46. Karátson, D. et al. Towards reconstruction of the lost Late Bronze Age intra-caldera island of
351 Santorini, Greece. Nature Sci. Rep **8**. (2018) https://doi/10.1038/s41598-018-25301-2.

352 47. Fabbro, G., Druitt, T.H., Scaillet, S. Evolution of the crustal magma plumbing system during
353 the build-up to the 22-ka caldera forming eruption of Santorini (Greece), *Bull Volcanol*. **75**:767
354 DOI 10.1007/s00445-013-0767-5 (2013).

355 48. Vakhrameeva, P. et al. The cryptotephra record of the Marine Isotope Stage 12 to 10 interval
356 (460-335 ka) at Tenaghi Philippon, Greece: Exploring chronological markers for the Middle
357 Pleistocene of the Mediterranean region. Quat. Sci. Rev. 200, 313–333. (2018)

Main Text Diagrams

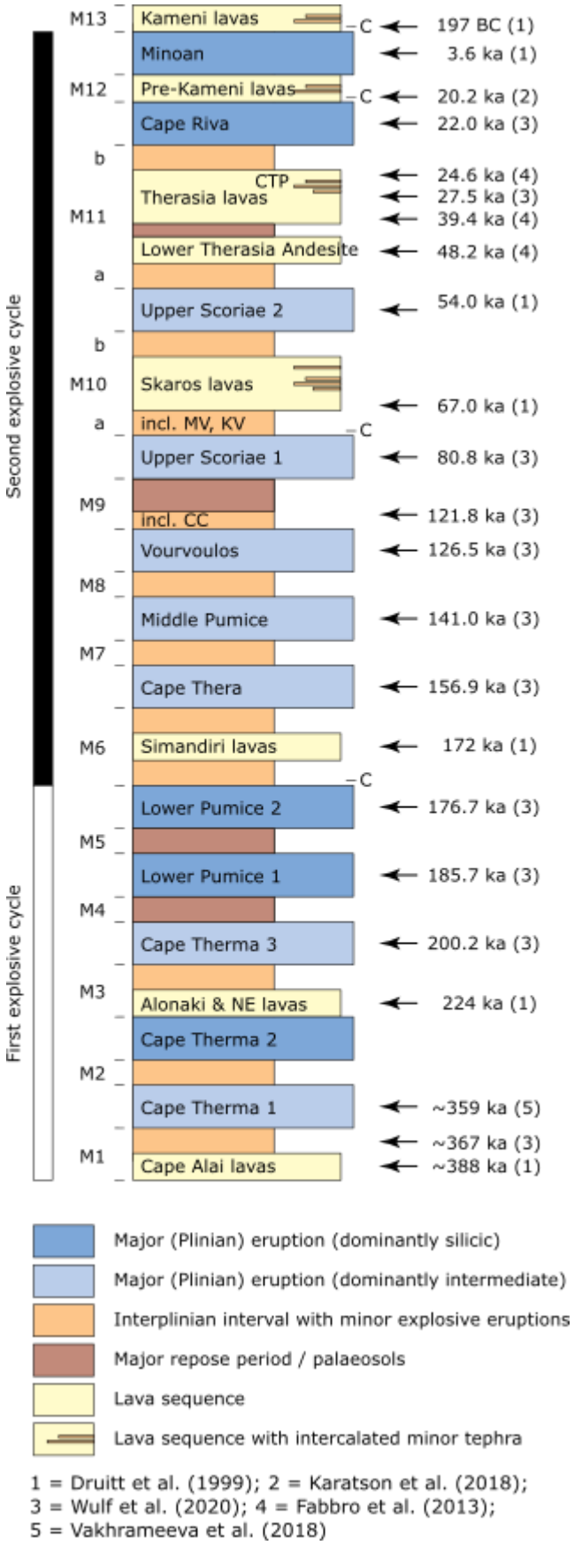

Figure 1. Stratigraphy and eruption chronology of Santorini from ~360 ka to the present, showing the twelve major explosive (Plinian) eruptions of Santorini (blue boxes) and divided into two explosive cycles. Episodes of caldera formation are marked by "C". Interplinian intervals (M1 to M13) are characterized by minor explosive eruptions, cinder cones/tuff rings (MV = Megalo Vuono cinder cone; KV = Kokkino Vuono cinder cone; CC = Cape Columbos tuff ring), lava sequences (lava flows, shields and domes), and major repose periods marked by palaeosols or weathering horizons. Deposits from minor explosive eruptions, including the widespread Cape Tripiti Pumice (CTP) within the Therasia dome complex, and palaeosols which mark major periods of repose also occur within the major lava sequences. Dates citations: 1[25]; 2[46]; 3[22]; 4[46]; 5[48].

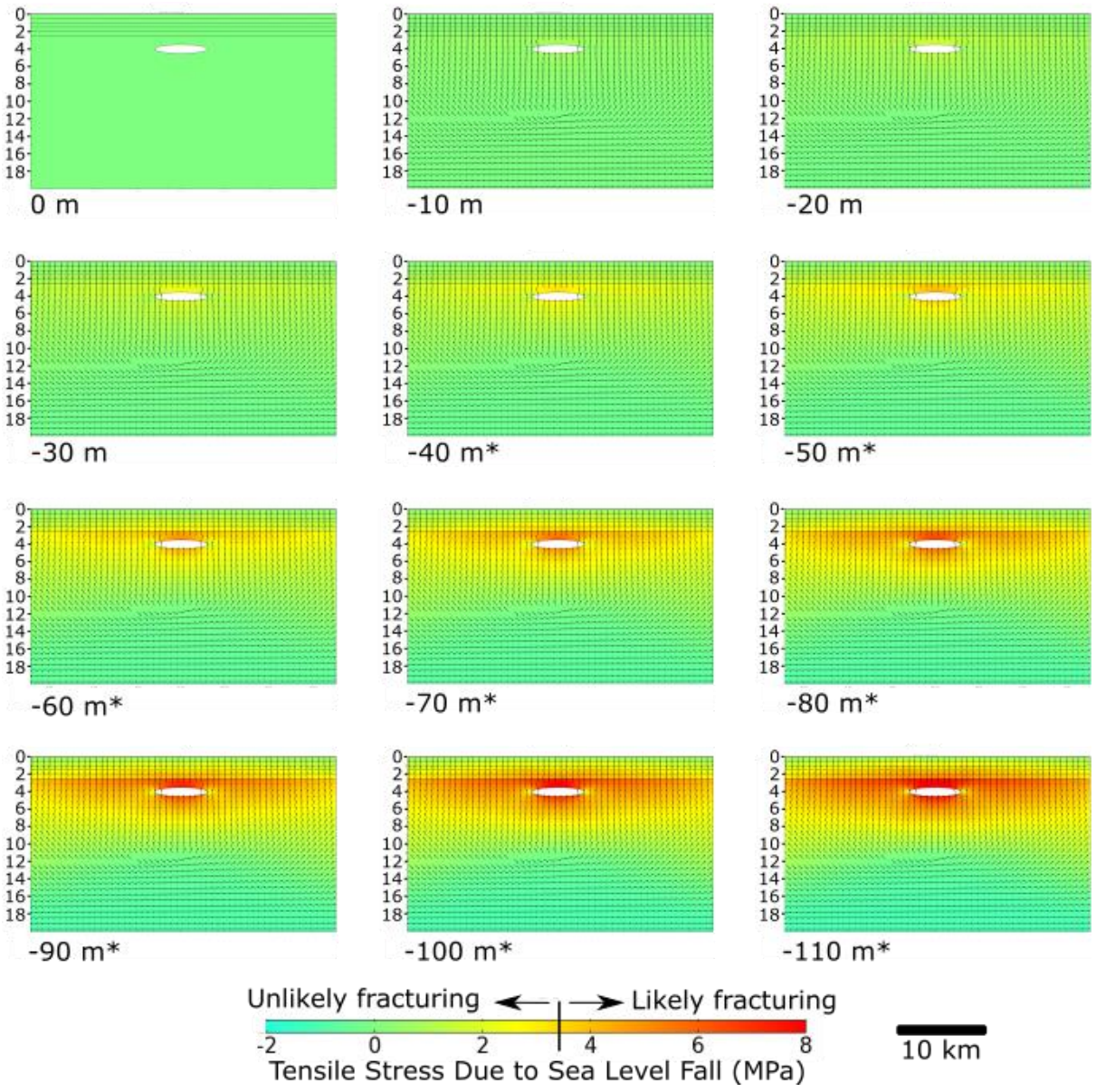

Figure 2. Numerical model of the increase in tensile stress around Santorini's shallow magma chamber (white elliptical hole) induced by sea-level fall in 10 m increments. Vertical scale indicates km below the surface. Red and yellow/orange areas indicate locations where tensile stress is likely to encourage dyke injection. Models with sea-level at -40 m (below the present level) or lower yield tensile stresses of > 3.5 MPa (the average crustal tensile strength), encouraging rupture of the magma-chamber roof and dyke injections. Initially (i.e. at -40 m), the induced tensile stress are limited to the margins of the chamber (host rock close to the chamber), so that the dykes would propagate only for a short distance and then become arrested. As the sea-level continues to fall the induced tensile stress spreads throughout the roof. When the sea-level has reached -70 m to -80 m, induced tensile stress occurs in much of the roof, whereby the first feeder-dykes in the sea-level cycle are generated (cf. Fig. 3). As the sea-level falls further towards the minimum of around -110 m, the entire roof of the magma chamber becomes subject to induced tensile stress, encouraging many

dyke-fed eruptions. Model geometry: the magma chamber centre is at 4 km depth below surface (consistent with geophysical evidence[34,35,41,42], the chamber width (horizontal dimension) is 6 km, and the chamber thickness (vertical dimension) is 1 km. The lateral edges of the model (out of shown view) are at 50 km either side of the centre of the chamber to avoid edge effects. There are 5 layers above the magma chamber, each 500 m thick, whose Young's moduli are as follows: First (surface) layer 5 GPa, second layer 10 GPa, third layer 15 GPa, fourth layer 20 GPa, and fifth layer 30 GPa. The layer/unit hosting the magma chamber has a Young's modulus of 40 GPa. The abrupt increase in Young's modulus between the fifth layer and the layer hosting the chamber is the reason for the notable tensile-stress concentration under the contact between these layers (the stress concentrates in the stiff layer/unit hosting the chamber). Full parameters are disclosed in the Methods section.

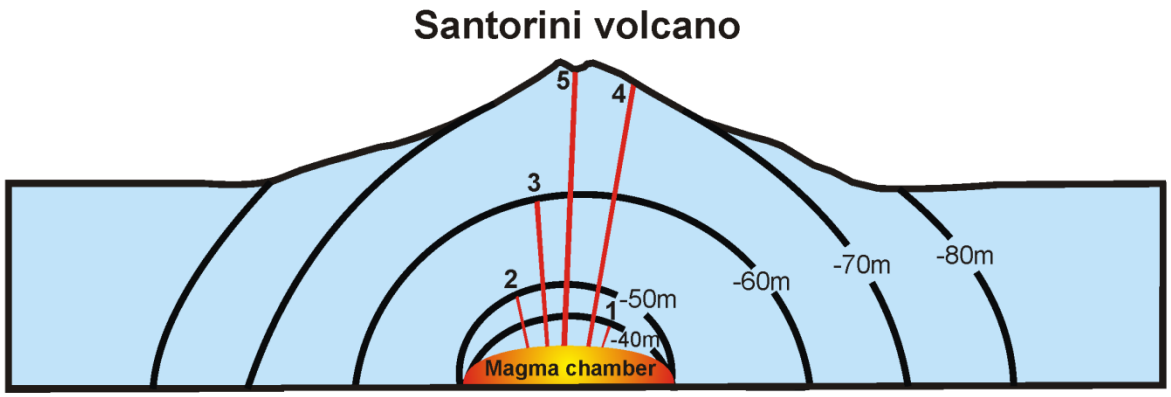

Figure 3. Schematic illustration of the spreading of the sea-level induced tensile stress in the roof of the magma chamber of the Santorini volcano and its effect on the propagation of injected dykes. The limits of the zones (marked by thick black semi-circular/semi-elliptical curves) within which induced tensile stresses favour dyke propagation for a given sea-level are indicated. The indicated sea-levels below the present one are -40 m, -50 m, -60 m, -70 m, and -80 m. Schematic propagation paths of five dykes (red straight lines), numbered 1 to 5, are shown. When the sea-level has fallen to -40 m, induced tensile stress is limited to a semi-elliptical zone close to the chamber (the outer boundary of the zone is the -40 m curve) and all injected dykes (represented by dyke 1) become arrested. When the sea-level falls further, tensile stress spreads through the roof of the chamber, but at levels -50 m and -60 m the outer boundaries of the high-tensile stress zones are still well below the surface, so that injected dykes (represented by dykes 2 and 3) become arrested. However,

when the sea-level falls to -70 m and, particularly, -80 m, induced tensile stresses reach to the surface of the volcano, and dyke-fed eruptions (represented by dykes 4 and 5) begin.

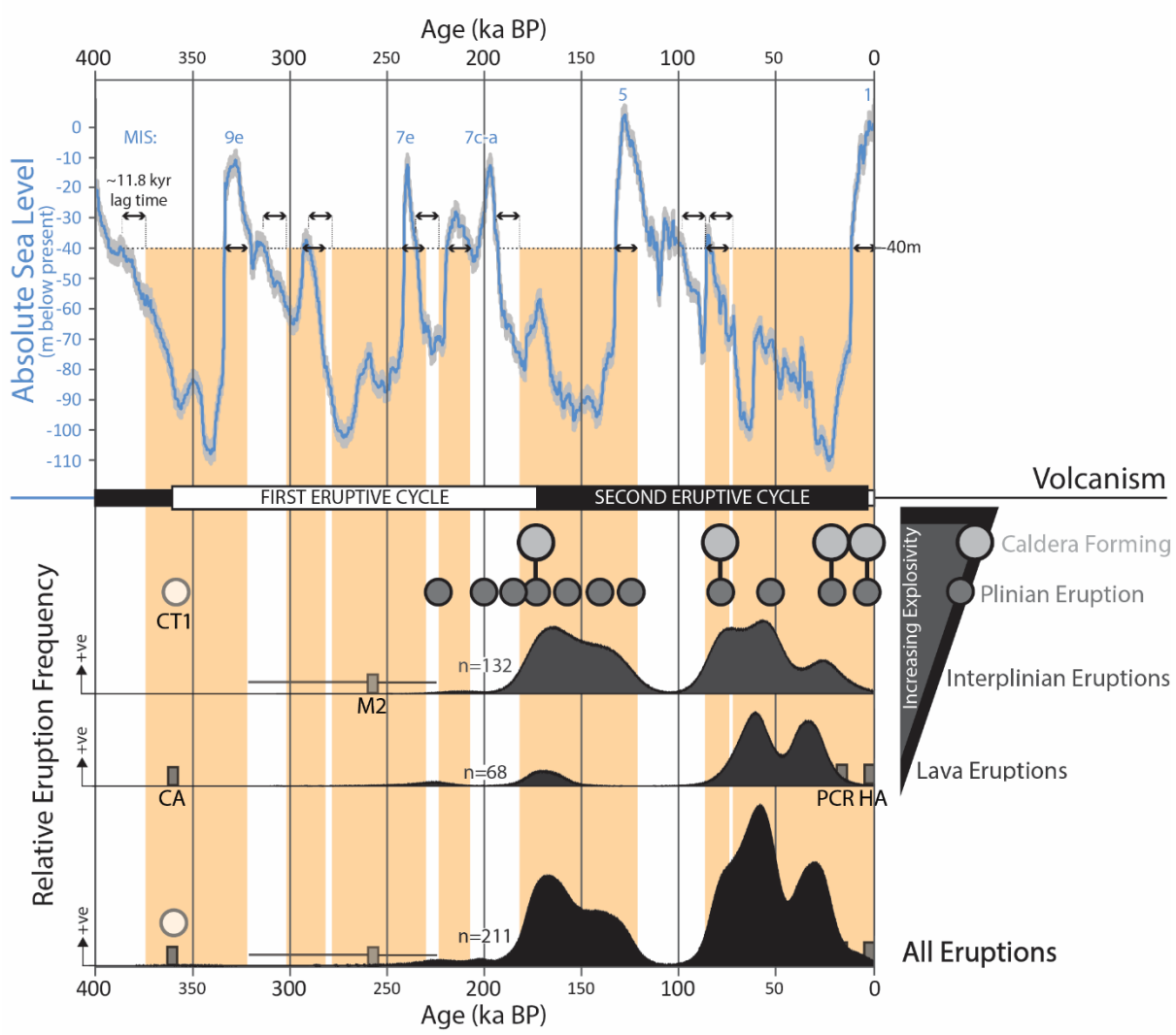

Figure 4. Santorini's eruptive stratigraphy (lower panels) aligned to the P_{max} absolute sea-level (blue curve with grey 95% confidence interval)[23,24]. Where both the chronology and the number of eruptions are well constrained, the eruption time series (lower half of diagram) is represented by kernel density estimates (grey/back) with the number of events of each type shown (total n=211). Where the number of events is either difficult to determine or the dating is very imprecise, eruptive events have been represented in grey boxes or circles (most likely date) with whiskers for the error (if known). The height of the boxes does not imply the number of events. These events are labelled to allow simple reference to the existing literature; CT1= Cape Therma 1, CA=Cape Alai Lavas, M2= interplinian deposits[44,45]. PCR=Post Cape Riva lavas and HA= Historical Activity. An estimation (~11.8 +/- 1.9 kyr) of the time-lag between sea-level passing through -40 m and the beginning of dyke-fed eruptions (at the sea-level of -70 m to -80 m) has been defined using the difference between the start and end of the period of eruptive activity between the Lower Pumice 2 eruption at 176.70 +/-

437 0.59 ka and the M9-2 eruption at 121.83 +/- 2.90 ka, and the times at which sea-level passes through
438 -40 m (see text for full explanation). This estimate is then tested over the rest of the time series
439 (vertical beige boxes). Also shown are the time periods of the eruptive 'cycles' which are traditionally
440 used to describe the cycles in composition and style of Santorini's eruptions.